Direct Probes of 4 nm Diameter Gold Nanoparticles Interacting with Supported Lipid Bilayers

Julianne M. Troiano,[†] Laura L. Olenick,[†] Thomas R. Kuech,[‡] Eric S. Melby,[‡] Dehong Hu,[⊥] Samuel E. Lohse,[∥] Arielle C. Mensch,[§] Merve Dogangun,[†] Ariane M. Vartanian,[∥] Marco D. Torelli,[§] Eseohi Ehimiaghe,[†] Stephanie R. Walter,[†] Li Fu,[⊥] Christopher R. Anderton,[⊥] Zihua Zhu,[⊥] Hongfei Wang,[⊥] Galya Orr,[⊥] Catherine J. Murphy,[∥] Robert J. Hamers,[§] Joel A. Pedersen,*[,‡,§] and Franz M. Geiger*[,†]

[†]Department of Chemistry, Northwestern University, 2145 Sheridan Road, Evanston, Illinois 60208, United States

[‡]Environmental Chemistry and Technology Program and [§]Department of Chemistry, University of Wisconsin, 680 North Park Street, Madison, Wisconsin 53706, United States

[∥]Department of Chemistry, University of Illinois at Urbana−Champaign, 600 S. Mathews Ave., Urbana, Illinois 61801, United States

[⊥]Environmental Molecular Sciences Laboratory, Pacific Northwest National Laboratory, Richland, Washington 99352, United States

S *Supporting Information*

ABSTRACT: This work presents molecular-level investigations of how well-characterized silica-supported phospholipid bilayers formed from either pure DOPC or a 9:1 mixture of DOPC:DOTAP interact with positively and negatively charged 4 nm gold metal nanoparticles at pH 7.4 and NaCl concentrations ranging from 0.001 to 0.1 M. Second harmonic generation (SHG) charge screening measurements indicate the supported bilayers carry a negative interfacial potential. Resonantly enhanced SHG measurements probing electronic transitions within the gold core of the nanoparticles show the particles interact irreversibly with the supported bilayers at a range of concentrations. At 0.1 M NaCl, surface coverages for the particles functionalized with the negatively charged ligand mercaptopropionic acid (MPA) or wrapped in the cationic polyelectrolyte poly(allylamine) hydrochloride (PAH) are estimated from a joint analysis of QCM-D, XPS, AFM, and ToF-SIMS to be roughly 1×10^7 and 1×10^{11} particles cm^{-2}, respectively. Results from complementary SHG charge screening experiments point to the possibility that the surface coverage of the MPA-coated particles is more limited by interparticle Coulomb repulsion due to the charges within their hydrodynamic volumes than with the PAH-wrapped particles. Yet, SHG adsorption isotherms indicate that the interaction strength per particle is independent of ionic strength and particle coating, highlighting the importance of multivalent interactions. ¹H NMR spectra of the lipids within vesicles suspended in solution show little change upon interaction with either particle type but indicate loosening of the gold-bound PAH polymer wrapping upon attachment to the vesicles. The thermodynamic, spectroscopic, and electrostatic data presented here may serve to benchmark experimental and computational studies of nanoparticle attachment processes at the nano−bio interface.
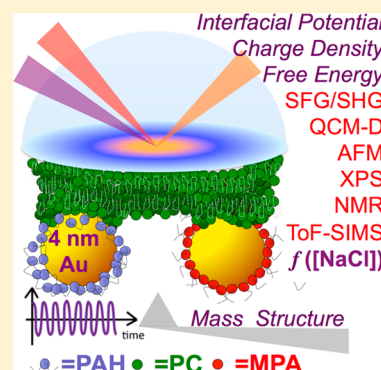
I. INTRODUCTION

Supported lipid bilayers serve as important models for probing binding interactions without the need for competitive binding assays.[1−6] They have proven particularly useful for elucidating interactions between nanoparticles and cell membranes in interfacial biological environments that are now collectively referred to as the nano−bio interface,[7,8] an emerging area of research spanning nanotechnology, biology, environmental science, and chemistry. While the interactions at aqueous/lipid bilayer interfaces are often driven by electrostatics, experimental quantification of interfacial charge densities and potentials is difficult, even when using scanning probes,[9] labels,[10] or conducting substrates.[11] This problem is compounded if one wishes to probe how lipid bilayers interact with nanoparticles. Quartz crystal microbalance (QCM), scanning

probe,[12−14] or surface plasmon resonance[15] approaches have been used to monitor changes in total mass coupled to a surface or dielectric constants in the interfacial region, but direct label-free methods that probe either a nanoparticle- or bilayer-specific property have largely been restricted to microscopic techniques that require ultrahigh-vacuum conditions,[16,17] under which volatile species are lost and drying effects may dominate the experimental outcome.

Given that a single "silver bullet" method for probing the nano−bio interface is not available at this time, combinations of complementary experimental techniques are needed if one

wishes to understand, control, and predict binding interactions at biological membranes. Here, we take a step in that direction by synchronizing nanoparticle and bilayer synthesis with second harmonic and vibrational sum frequency generation (SHG and SFG) measurements with QCM with dissipation monitoring (QCM-D), fluorescence, nuclear magnetic resonance (NMR) spectroscopy, X-ray photoelectron spectroscopy (XPS), atomic force microscopy (AFM), and time-of-flight secondary ion mass spectrometry (ToF-SIMS) measurements across multiple laboratories. First, we show that well-characterized phosphatidylcholine (PC)-rich lipid bilayers supported on fused silica carry a sizable negative interfacial potential at pH 7.4. Second, we probe how the supported lipid bilayers, as well as vesicles suspended in solution, interact with spherical 4 nm gold metal nanoparticles (AuNPs), which are chosen because of chemical stability, ease of functionalization, and their high potential for use in biomedical applications.[18,19] We provide estimates for absolute surface coverages and interaction strengths for particles that are either functionalized with the negatively charged ligand mercaptopropionic acid (MPA) or wrapped in the cationic polyelectrolyte poly(allylamine) hydrochloride (PAH). Finally, we discuss the results in the context of a mechanism in which the attached MPA-AuNPs contain a higher charge density and are therefore subject to increased interparticle charge−charge repulsion within their hydrodynamic volume than the attached PAH-AuNPs. The overall energetics of attaching an individual AuNP to the bilayer are found to be driven by multivalent interactions that appear to be largely independent of ionic strength and particle coating.

II. EXPERIMENTAL METHODS

II.A. Bilayer Preparation. In the experiments, we used 1,2-dimyristoyl-*sn*-glycero-3-phosphocholine (DMPC), 1,2-dimyristoyl-*sn*-glycero-3-phospho-(1-*rac*-glycerol) (DMPG), 1,2-dioleoyl-*sn*-glycero-3-phosphocholine (DOPC), and 1,2-dioleoyl-3-trimethylammonium-propane (DOTAP, all from Avanti Polar Lipids, Figure 1), chosen for their contrasting phase
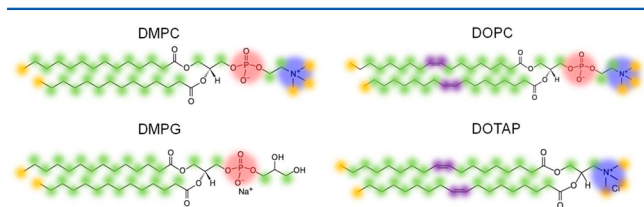

Figure 1. Molecular structure of the lipids used in this work. C−H stretches (orange, green, and purple) are probed by SFG. Interfacial potentials set up by positive (blue) and negative (red) charges are probed by SHG.

transition temperatures, their differing charge states, and the biological relevance of the PC headgroup.[20] As described in detail in the Supporting Information, we prepared lipid bilayers from small unilamellar vesicles of pure DOPC as well as from lipid mixtures containing 90% DOPC or DMPC and 10% positively or negatively charged lipids. Small unilamellar lipid vesicles, prepared by extrusion though a 0.05 μm membrane filter (Avanti, 610000), exhibited ζ potentials of -4 ± 3, -5 ± 1, and -2 ± 1 mV for pure DOPC in 0.1, 0.01, and 0.001 M NaCl buffered to pH 7.4 with 0.01 M Tris. ζ potentials of $+10 \pm 2$, $+22 \pm 4$, and $+31 \pm 4$ mV were obtained for the 9:1 mixtures of DOPC:DOTAP at 0.1, 0.01, and 0.001 M NaCl, respectively, at pH 7.4. Corresponding values for the 9:1

mixtures of DMPC:DMPG were -12 ± 1, -19 ± 2, and -18 ± 2 mV for 0.1, 0.01, and 0.001 M NaCl at pH 7.4.

Substrate supported lipid bilayers were assembled by vesicle fusion,[21] and experiments were carried out at room temperature (24−26 °C). All bilayers were formed at 0.1 M NaCl (in the presence of 0.005 M CaCl$_2$ for DMPC:DMPG bilayers). For the particle adsorption experiments conducted at 0.001 and 0.01 M NaCl, we lowered the salt concentration to the desired value prior to introduction of nanoparticles. As detailed in the Supporting Information, the mass of the supported lipid bilayers was calculated using a Voigt−Kelvin viscoelastic model[22] from changes in frequency and energy dissipation measured by QCM-D. The topography of the bilayer was assessed by tapping mode AFM. The electrostatic and structural properties of the bilayers were probed by second harmonic and vibrational sum frequency generation (SHG and SFG) using our previously published approach,[23−26] with modifications as detailed in the Supporting Information. To assess the fluidity of the supported lipid bilayers, fluorescence recovery after photobleaching (FRAP) was carried out using PC lipids tagged with TopFluor on an inverted laser scanning confocal fluorescence microscope (LSM 710, Zeiss) using 488 nm laser excitation and acquiring emission images at 500−550 nm at a 230 ms frame rate. Lipid diffusion coefficients within the bilayers were assessed at 0.1 M NaCl and pH 7.4 (0.01 M Tris).

II.B. Gold Nanoparticle Synthesis, Functionalization, and Characterization. For our experiments, we synthesized, purified, and characterized 4 nm AuNPs functionalized with poly(allylamine) hydrochloride (PAH) or mercaptopropionic acid (MPA). Briefly, 4 nm citrate-stabilized AuNPs were prepared by direct reduction in aqueous solution, as were 4 nm MPA-AuNPs.[27−29] PAH-AuNPs were prepared by wrapping citrate-stabilized AuNPs using a polyelectrolyte deposition approach.[30] The PAH-AuNPs were subsequently purified by centrifugation and washing (7500g, 90 min). The MPA-AuNPs were purified by diafiltration using 20 volume equivalents of nanopure deionized water. We characterized the purified AuNPs by UV−vis absorption spectroscopy, transmission electron microscopy (TEM), dynamic light scattering (DLS), laser-Doppler microelectrophoresis, and XPS; the complete characterization data are provided in the Supporting Information, specifically Figures S1 and S2. The diameters of the AuNP cores were determined in solution by UV−vis to be ~3.5 nm,[31] and TEM size analysis indicated that the PAH-AuNPs possessed a core diameter (d_{core}) of 4.5 ± 1.4 nm (n = 1085). ζ potentials of the PAH-AuNPs determined at pH 7.4 (0.01 M Tris buffer) and at 0.001 and 0.1 M NaCl were +38 ± 3 and +32 ± 2 mV, respectively, and their number-averaged hydrodynamic diameter at 0.001 M NaCl was found to be 6 ± 2 nm and ranged between 20 and 80 nm (Figure S2D) at 0.1 M NaCl. XPS analysis indicated that about four PAH polymer strands are associated with each AuNP. With ~15 kDa/polymer we find that each particle is associated with ~4000 ammonium groups, along with a number of counterions that depends on the ionic strength.

For the MPA-AuNPs, d_{core} was 4.2 ± 1.2 nm (n = 613).[32] ζ potentials of the negatively charged MPA-AuNPs determined at pH 7.4 (0.01 M Tris) and 0.001 and 0.1 M NaCl were −29 ± 1 and −27 ± 2 mV, respectively, and their number-averaged hydrodynamic diameter at 0.001 M NaCl was found to be 9 ± 2 nm. At 0.1 M NaCl, the number-averaged hydrodynamic diameter of the MPA-AuNPs increased from between 100 to

400 nm to between 420 and 450 nm over the course of 2 h (Figure S2C). UV–vis spectra (Figure S2) indicate that for 10 nM MPA- or PAH-AuNPs maintained at 0.1 M NaCl and pH 7.4 (0.01 M Tris), the electronic properties of the particles do not change much over the course of 150 min, whereas measurements of the hydrodynamic diameters indicate that the MPA-AuNPs aggregate.

II.C. NMR Spectroscopy of Vesicles and AuNPs. ^{1}H NMR spectra were acquired in D_2O using a Varian Unity Inova 500 MHz narrow bore spectrometer. For samples containing residual water, the large water peak was suppressed using presaturation. Unless stated otherwise, the presaturation delay for aqueous samples was 2 s and the acquisition time was 1 s, with a four-step purge. The number of scans for each sample was 128 or 256, depending on the signal-to-noise ratio. All NMR spectra were processed using MNova NMR software. Lipid vesicles were prepared by extrusion as described above, except that lipids were rehydrated in Tris buffer solution in D_2O (0.1 M NaCl, 0.01 M Tris, pD 7–8). Lipid vesicles (12 mM) and PAH-AuNP (10 nM particle concentration) or free PAH polymer (10 nM) were agitated in an NMR sample tube for 10 s and then allowed to interact at room temperature for 2 h before NMR acquisition.

III. RESULTS

III.A. Supported Lipid Bilayers Are in a Fluid State As Probed by FRAP Measurements and Structurally Invariant with Ionic Strength As Probed by SFG. Figure 2A shows that the final acoustic masses obtained following
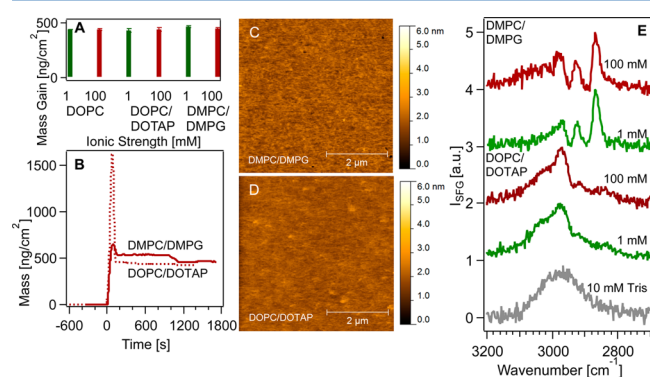

Figure 2. (A) Total acoustic mass gain, evaluated by QCM-D, for conditions indicated. (B) Formation of supported lipid bilayers from vesicles formed from 9:1 mixtures of DMPC/DMPG (solid line) and DOPC/DOTAP (dashed line) probed by QCM-D at 0.1 M NaCl. The small decrease in mass in the 9:1 DMPC:DMPG bilayer commencing at 1000 s is most likely due to the removal of loosely attached intact vesicles during rinsing with Ca^{2+}-free solution. (C, D) AFM ($5 \times 5 \, \mu m^2$) images of bilayers formed from DMPC/DMPG and DOPC/DOTAP at 0.1 M NaCl. (E) Normalized ssp-polarized SFG spectra of supported lipid bilayers at pH 7.4 and in the presence of 0.01 M Tris (gray) for 0.001 M (green) and 0.1 M (red) NaCl using vesicles formed from 9:1 DMPC/DMPG (top pair) and DOPC/DOTAP (bottom pair) mixtures.

formation of each bilayer type are invariant with [NaCl] and correspond to lipid surface coverages that range from ~3.4 to $4.1 \times 10^{14} \, cm^{-2}$, in agreement with reported values for well-formed supported lipid bilayers.[33,34] Figure 2B shows that the change in acoustic mass detected by the QCM-D sensor follows the well-established vesicle-rupture mechanism[35] that involves a large mass gain until a critical vesicle coverage is attained,

followed by a partial mass loss as vesicles rupture and fuse to form a supported lipid bilayer. AFM images (Figure 2C,D) of the surfaces after bilayer formation show smooth surfaces with some topographic height variations mirroring those of the underlying SiO_2 film (consistent with prior reports)[36] and confirm that the vesicles have fused to form lipid bilayers. FRAP measurements indicate diffusion coefficients at 26 °C for TopFluorPC of $1.7 \pm 0.3 \, \mu m^2/s$ for the bilayers formed from DMPC/DMPG, $1.8 \pm 0.4 \, \mu m^2/s$ for the bilayers formed from DOPC/DOTAP, and $2.1 \pm 0.6 \, \mu m^2/s$ for those formed from pure DOPC. These results are consistent with the presence of well-formed bilayers in the fluid state. Moreover, the mobile fraction for all three systems exceeded 85%, in agreement with previous reports for fluid solid-supported lipid bilayer systems.[37−40]

We then applied vibrational SFG spectroscopy to probe for structural changes along the carbon backbone and the methyl groups of the headgroups of phospholipids comprising the supported lipid bilayers as they were subjected to salt concentrations of 0.001, 0.01, and 0.1 M at pH 7.4 in the presence of 0.01 M Tris buffer, as those electrolyte concentrations were applied in the studies aimed at quantifying the interfacial electrostatics (*vide infra*). As shown in Figure 2E, we find that the SFG spectra obtained from both types of bilayers are largely invariant with salt concentration over the range studied, indicating that structural rearrangements within the lipid alkyl chains, as probed by SFG in the C–H stretching region, are negligible under these experimental conditions. These spectra were recorded using the ssp polarization combination, which is sensitive to those components of vibrational transition dipole moments oriented perpendicular to the interface. SFG spectra shown in the Supporting Information indicate variations of ±30% in the intensities of the various vibrational modes. Details regarding spectroscopic assignments, and the role of Tris buffer, are presented in the Supporting Information as well.

III.B. Supported Lipid Bilayers Surveyed Produce a Negative Interfacial Potential. Having verified the integrity of the lipid bilayers using a variety of experimental techniques, we characterized the interfacial potential, ϕ_0, and charge densities, σ_0, associated with the supported lipid bilayers using the Eisenthal $\chi^{(3)}$ method (Figure 3). This variant of SHG is based on the second-order polarization of interfacial water molecules in the presence of an interfacial potential, ϕ_0.[41,42] Intuitively, the method can be thought of as an optical voltmeter in which the SHG response is proportional to ϕ_0,[24]
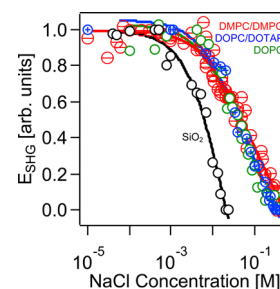

Figure 3. Normalized SHG response (symbols) and Gouy–Chapman fits (lines) as a function of NaCl concentration at pH 7.4 and 0.01 M Tris buffer for plain fused silica (black ○) and bilayers prepared from pure DOPC (green ○) and 9:1 mixtures of DOPC/DOTAP (blue ⊕) and DMPC/DMPG (red ⊖).

which is obtained by integrating the electrostatic potential, $\phi(\zeta)$, from the interface ($z = 0$) to infinity ($z = \infty$). In other words, the interfacial potential we report here is for zero distance from the silica surface and referenced to the potential in the bulk solution (0 V).

Before presenting the experimental results, we briefly discuss some considerations that are important when applying the Eisenthal $\chi^{(3)}$ method to supported lipid bilayers. First, changes in the salt concentration lead to changes in the ion diffusion potential across a supported lipid bilayer in ≥ 2 min.[2] Given that we collect our SHG data at a given salt concentration for approximately 15 min following a 5 min waiting period after changing the salt concentration, the interfacial potential we report here accounts for changes in the diffusion potential with changes in the salt concentration. Figure 2E shows that the SFG spectra of the bilayers studied here are invariant with salt concentration. This finding is consistent with the notion[2] that the magnitude of the permanent dipoles formed predominantly by the lipid alkyl chains within the bilayer is independent of salt concentration. While the field due to the permanent dipoles should sum to zero under ideal conditions, we caution that any residual nonzero bilayer potential due to bilayer asymmetry[43,44] induced in the presence of the underlying charged fused silica substrate may contribute to ϕ_0 in a minor fashion.

Second, the SHG signal intensity (I_{SHG}) has been shown experimentally to decline when ϕ_0 at negatively charged surfaces becomes more positive[45,46] and to increase when ϕ_0 decreases at positively charged surfaces.[46,47] This experimental observation is generally interpreted as follows: changes in ϕ_0 cause changes in the I_{SHG} according to the polarization (or, intuitively, the up or down alignment, even though we caution that dipolar alignment is not the only determinant in the $\chi^{(3)}$ effect) of the water dipole moments within the SHG active interfacial region that are subject to ϕ_0. While computational approaches have indicated that quadrupole contributions may be important for SHG signals produced at uncharged air/liquid interfaces,[48] those contributions are independent of the direction of the water dipole moments and would not produce the experimental outcomes observed at charged aqueous/solid interfaces.

Third, recent nonlinear optical studies have shown qualitatively that the polarization of interfacial water molecules depends on the chemical identity and charge of the headgroups of lipid monolayers at the air/water interfaces. Specifically, heterodyne-detected SFG spectra[49,50] and molecular dynamics simulations[51] indicate that, on average, water molecules interacting with zwitterionic headgroups of phospholipid monolayers at the air−water interface point their oxygen atoms toward the bulk aqueous phase as if they interacted with a negatively charged silica surface (albeit to a smaller extent). Preferential hydroxide ion adsorption has been invoked to rationalize the observation of negative ζ potentials over bilayers prepared from zwitterionic lipids at pH $\gtrsim 4$.[52] However, similar to what has been reported for the case of Cl$^-$ ions,[9] OH$^-$ may not have a large enough binding interaction with the PC headgroup, and the effect could be due to the orientation and the binding strengths of water molecules to the phosphate and trimethylammonium ends of the of the permanent dipole of the zwitterionic headgroup.[49−51] In our system, the pure bilayers are formed from zwitterionic DOPC, and lipids with PC headgroups are the majority component in the bilayers formed from the lipid mixtures, making these literature precedents particularly relevant for interpreting our data.

If ϕ_0 emanating from the largely zwitterionic bilayers over the SiO$_2$ support were indeed negative, we would expect SHG signal intensities from the bilayers studied here to decrease with increasing [NaCl]. Figure 3 shows that this expectation is indeed met at pH 7.4 in 0.01 M Tris between 10^{-5} and 0.1 M NaCl. The interfacial charge density, and thus any apparent charge on the zwitterionic headgroups, is then obtained by fitting a suitable double-layer model to the SHG E-field vs [NaCl] plots. Recent spin-labeled[53] and scanning probe[9] studies as well as molecular dynamics simulations[54] have confirmed the appropriateness of Gouy−Chapman theory[55] for describing electrostatics within the electrical double layer over supported lipid bilayers that was put forth in earlier work by MacDonald and Bangham.[2] While taking care to not over-interpret the model, we apply Gouy−Chapman theory here in a fashion that accounts for the charges associated with the silica surface and the presence of Tris buffer, as detailed below.

We recently reported SHG salt screening data for the fused silica/water interface maintained at pH 7 that resulted in an interfacial charge density of -0.013 ± 0.002 C/m^2.[56,57] As shown in the Supporting Information, we fit the Gouy−Chapman model to the fused silica data shown in Figure 3, where 0.01 M Tris is present, and find an additional charge density of $+0.009$ ($+0.003/-0.001$) C/m^2 due to adsorbed TrisH$^+$ cations that must be taken into account. Assuming the interfacial species is TrisH$^+$, we calculate that 6 ($+2/-1$) $\times 10^{12}$ buffer cations are present per cm^2 at the fused silica/water interface. Taking the sum of the charge densities for the fused silica and the TrisH$^+$ (i.e., assuming that the TrisH$^+$ cations remain in the water layer between the fused silica substrate and the proximal leaflet of the bilayer), we then apply the Gouy−Chapman model, with the interfacial potential referenced to that of the bulk aqueous phase (0 V, *vide supra*), to obtain the charge density of the bilayers as the average of the distal and proximal leaflets of the bilayer. This analysis yields charge densities of -0.011 ($+0.003/-0.005$) C/m^2 for pure DOPC bilayers, -0.015 ($+0.003/-0.004$) C/m^2 for bilayers formed from the 9:1 mixture of DOPC/DOTAP, and -0.024 ($+0.003/-0.005$) C/m^2 for bilayers formed from the 9:1 mixture of DMPC/DMPG. We conclude that following the subtraction of the interfacial charge density of the bare fused silica/water interface and that of TrisH$^+$ at pH 7.4, the bilayers studied here are associated with apparent negative interfacial charge densities that are largely indistinguishable from one another. Given that the majority component of the bilayer is a zwitterionic lipid, this finding is not surprising.

Given the evidence from SFG spectroscopy (bottom spectrum in Figure 2E), it is likely that TrisH$^+$ is present at the surface in our DOPC/DOTAP bilayer experiments. Yet, the TrisH$^+$ surface coverage may be less when compared to the case of the DMPC/DMPG bilayers because of Coulombic repulsion between TrisH$^+$ and the positively charged TAP headgroup. Given that both bilayers contain 90% zwitterionic PC headgroups, the changes in TrisH$^+$ surface coverage for the various bilayer systems studied here are probably minor.

Provided that each lipid occupies an area of 0.72 nm^2,[2,58] we calculate that each zwitterionic headgroup of the bilayer formed from pure DOPC is associated with an apparent charge of -0.028 ($+0.008/-0.007$) $\times 10^{-19}$ C, corresponding to $1.8 \pm 0.5\%$ of an elementary negative charge. Our estimate depends on the headgroup size but is in reasonable agreement with that reported using scanning probes,[9] given the differences in ionic strength, bilayer composition, and substrate.
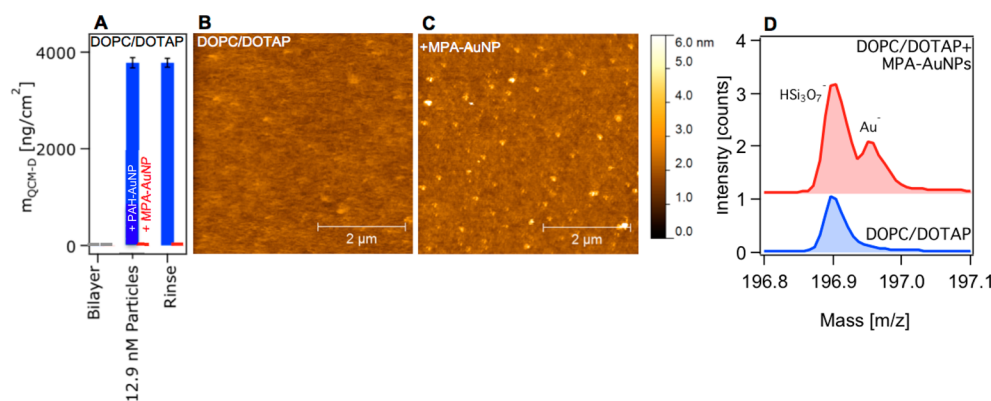
Figure 4. (A) Acoustic mass gains determined by QCM-D upon 60 min exposure of a supported lipid bilayer formed from a 9:1 mixture of DOPC and DOTAP to 12.8 nM positively charged PAH-coated and negatively charged MPA-coated 4 nm spherical AuNPs in 0.01 M Tris buffer and 0.1 M NaCl at pH 7.4. (B, C) Topography image of bilayers formed from a 9:1 mixture of DOPC and DOTAP in 0.01 M Tris, 0.1 M NaCl, pH 7.4, on an ultraflat thermal SiO$_2$ substrate wafer before (B) and after (C) exposure to MPA-AuNPs (10 nM). Images from the same experiment carried out on a freshly prepared bilayer and adjusted to the same scale. (D) Normalized ToF-SIMS spectra of 9:1 DOPC:DOTAP bilayer before (bottom) and after (top) interaction with 1 nM MPA-AuNPs at room temperature and in 0.1 M NaCl and pH 7.4 (0.01 M Tris buffer) and subsequently rinsed with buffer. Bilayer samples were prepared in and then removed from the flow cell following rinsing and allowed to dry prior to analysis.

III.C. Positively and Negatively Charged Nanoparticles Interact with Supported Lipid Bilayers Rich in DOPC. The apparent negative interfacial potentials carried by SiO$_2$-supported bilayers formed from the largely zwitterionic phospholipids led us to test their interaction with AuNPs functionalized with oppositely charged ligands. We chose 4 nm positively and negatively charged spherical gold nanoparticles because of their stability, their potential biomedical applications,[18,59] and well-established methods for their synthesis, characterization, and functionalization.[59] As described in section II, positively and negatively charged particles were prepared by functionalizing them with the polyelectrolyte poly(allylamine) hydrochloride (PAH) and mercaptopropionic acid (MPA), respectively.

We monitor nanoparticle interactions with supported lipid bilayers first by tracking changes in acoustic mass using QCM-D (Figure 4A). The positively charged PAH-AuNPs show substantial and irreversible attachment (210 ± 20 Hz) to the DOPC/DOTAP bilayer, corresponding to acoustic masses of roughly 3.8 μg/cm^2 (or roughly 6 × 10^{12} particles attached per cm^2) at 0.1 M NaCl over 60 min and large changes in dissipation ((28 ± 2) × 10^{-6}) when compared to the 0.5 × 10^{-6} dissipation factors of both bilayers (changes in frequency and dissipation are shown in the Supporting Information). In contrast, the hour long exposure of supported lipid bilayers formed from the 9:1 mixture of DOPC/DOTAP to the MPA-coated particles at 12.8 nM concentration leads to acoustic masses at or near the detection limit (5 ng/cm^2, which corresponds to 5 × 10^9 AuNPs per cm^2). Likewise, dissipation factors show a small change of 0.5 × 10^{-6}. Complementary XPS experiments show no signal in the gold spectral region for this particle/bilayer combination, even at increased pass energy and signal averaging (detection limit on the order of 0.01 ng/cm^2 or 1 × 10^7 AuNPs per cm^2). Yet, Figure 4B,C shows AFM images of bilayers formed from a 9:1 mixture of DOPC and DOTAP before and after exposure to 12.8 nM of the negatively charged MPA-functionalized particles, at 0.1 M NaCl and 0.01 M Tris buffer, that indicate a sparse coverage of bright spherical features which are distinguished from intact vesicles attached to the bilayer by their heights of up to 15 nm above the bilayer. Complementary ToF-SIMS experiments carried out on the same system after rinsing with buffer and then drying shows ample signal intensity from gold at 196.95 amu (Figure 4D).

III.D. Evaluating Bilayer Integrity upon Nanoparticle Attachment. To assess the quality of the supported lipid bilayers after exposure to the nanoparticles, we carried out FRAP measurements using TopFluorPC. The diffusion coefficients for TopFluorPC were statistically indistinguishable before and after exposure to PAH- or MPA-AuNPs at concentrations of 0.1 and 10 nM ($p > 0.05$; Table S4). These results are again consistent with what we reported (*vide supra*) in the absence of the nanoparticles and indicate, again, the presence of well-formed bilayers that are in the fluid state following exposure to both types of nanoparticles at two different concentrations.[37−40]

III.E. Reversibility of Attachment. We then probed the interaction of the positively and negatively charged nanoparticles with the bilayer formed from a 9:1 mixture of DOPC/DOTAP by SHG with the expectation of probing the SHG-active transitions within the metal core[60] of nanoparticles directly at the aqueous/supported lipid bilayer interface. After rinsing away excess lipid vesicles with Tris buffer at 0.1 M NaCl, the SHG intensity was recorded at 300 ± 5 nm in the absence of nanoparticles. We typically obtain an average of 80 ± 10 counts/s for a bilayer at 0.1 M NaCl, 0.01 M Tris, and pH 7.4 when using pulse energy of 0.4 μJ, and this intensity level serves as a reference point for our experiments. Then, Tris buffer solutions containing increasing concentrations of gold nanoparticles in 0.1 M NaCl were injected into the sample cell, without rinsing with buffer between successive increases in particle concentration, and the SHG intensity was recorded near 300 nm after each injection until a steady signal was attained.

Figure 5A shows that the SHG intensity increases near 300 nm when the bilayers are exposed to PAH- and MPA-NPs at concentrations as low as 1 × 10^{-14} M, suggesting resonance enhancement of the SHG signal upon particle adsorption to the interface as an important SHG signal generation process in both cases. Studies described below verify the signals to be due to SHG and not fluorescence. The increases in the SHG intensity obtained upon addition of gold nanoparticles to the supported lipid bilayers may be attributable to the electronic
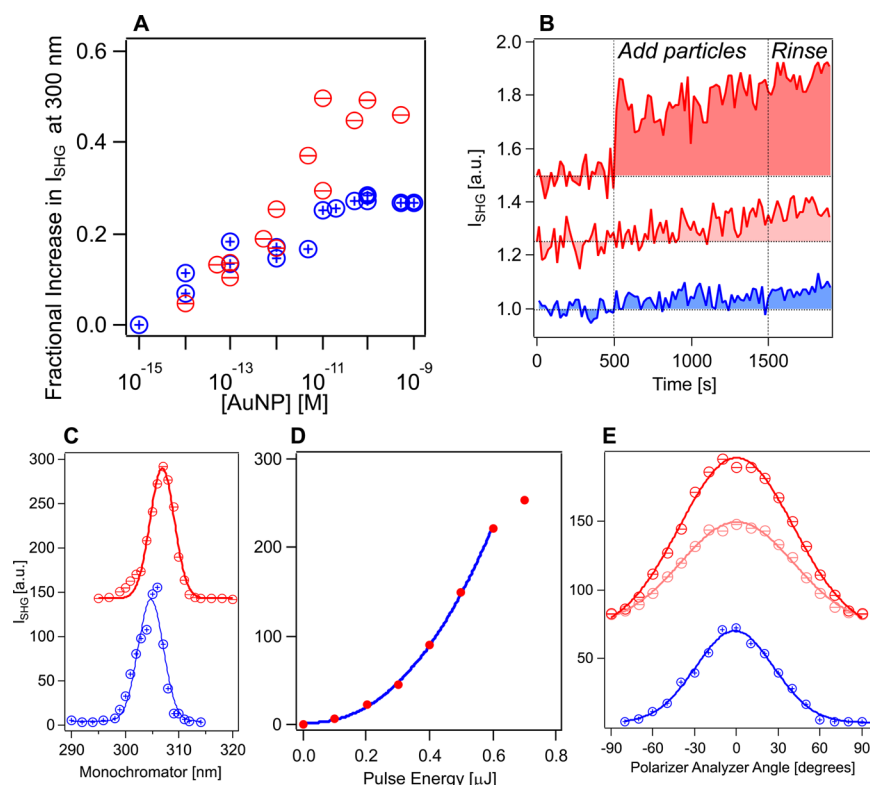
Figure 5. (A) SHG intensity as a function of nanoparticle concentration for a supported lipid bilayer formed from a 9:1 mixture of DOPC and DOTAP upon exposure to negatively charged MPA-AuNPs (red ⊖) and positively charged PAH-AuNPs (blue ⊕). p-in/all-out polarization combination, λ_{SHG} = 306 nm, 0.1 M NaCl and 0.01 M Tris buffer. Uncertainties on each SHG E-field is below 1% as given by the Poisson statistics of photon counting. Reproducibility of the experiments is assessed by performing the experiments in duplicate for the PAH-AuNPs and in triplicate for the MPA-AuNPs. See text for details. (B) SHG intensity as a function of time at 305 nm in the presence of a bilayer formed from a 9:1 mixture of DOPC and DOTAP in the presence of 10^{-9} M MPA (red, offset by 1.5), 10^{-11} M MPA (pink, offset by 1.25), and 10^{-11} M PAH (blue). At t = 500 s nanoparticles were introduced to the bilayer at 0.1 M NaCl and 0.01 M Tris. A buffer rinse was introduced to the bilayer system at t = 1500 s. (C) SHG intensity as a function of monochromator wavelength collected using the p-in/all-out polarization combination and Gaussian fit resulting in 3.2 ± 0.1 nm bandwidth for 0.1 nM concentration of PAH-coated (blue ⊕) and 3.1 ± 0.1 nm for 0.1 nM concentration of 4 nm MPA-AuNPs (red ⊖, offset by 140) interacting with a supported lipid bilayer formed from a 9:1 mixture of DOPC and DOTAP at 0.1 M NaCl and 0.01 M Tris buffer. Any departure from the Gaussian fit function is due to chirping of the pulse. (D) SHG intensity collected using the p-in/all-out polarization combination as a function of pulse energy at 612 nm for 1 nM concentration of PAH-coated 4 nm AuNPs interacting with a supported lipid bilayer formed from a 9:1 mixture of DOPC and DOTAP at 0.1 M NaCl and 0.01 M Tris buffer. Blue curve is a power function of the form $y = A + Bx^p$, where p = 2.28 ± 0.06. (E) SHG intensity at 306 nm collected as a function of polarizer analyzer angle while probing with p-polarized fundamental light for 0.1 nM concentration of PAH-coated (blue ⊕, bottom) and 10 pM (pink ⊖, offset by 80) and 1 nM (red ⊖, offset by 80) concentrations of 4 nm MPA-AuNPs interacting with a supported lipid bilayer formed from a 9:1 mixture of DOPC and DOTAP at 0.1 M NaCl and 0.01 M Tris buffer.

structure, quadrupole modes, or local field enhancement of the nanoparticles.[60,61] The relatively featureless absorption spectra in the 300 ± 20 nm tuning range that is readily accessible with the tunability of the optical parametric amplifier used in our setup make it difficult to verify unambiguously whether the SHG intensity increases are attributable to SHG resonance enhancement. Yet, while the interfacial potential produced in the presence of charged adsorbates,[45,61] in this case the charged ligands, lipids, and counterions, may contribute to the SHG process, the observation that the SHG signals increase for the positively charged and for negatively charged particles suggests that resonant enhancement contributes strongly to the SHG process in both cases.

Our comprehensive set of AFM, XPS, QCM-D, ToF-SIMS, and SHG experiments indicate that much fewer MPA-AuNPs attach to the supported lipid bilayers studied here than PAH-AuNPs. Indeed, we estimate from XPS that at 0.1 M NaCl concentration less than 0.01 ng/cm^2 particles, or just 1×10^7 4 nm AuNPs per cm^2, are attached to the supported lipid bilayer

formed from the 9:1 mix of DOPC:DOTAP, whereas the surface coverage is approximately 3.8 μg/cm^2 (or roughly 6×10^{12} particles attached per cm^2) for the PAH-coated particles under the conditions of the QCM-D experiments. Yet, the SHG signals produced by the attached MPA-coated particles are larger than those obtained from the attached PAH-coated particles, pointing to an in-phase, or constructive, interference between the resonantly enhanced and potential-dependent SHG terms. Destructive interference between the two terms probably suppresses SHG signal intensities in the case of the PAH-AuNPs, which produce less SHG signal intensity even though their surface coverages are several orders of magnitude above those we estimate for the MPA-AuNPs. This interpretation of the data is subject to the provision that the electronic properties relevant for the SHG process of nanoparticles, which can be assessed from their UV−vis absorption spectra, are largely invariant during the experiments, which control experiments shown in Figure S2 indicate to be the case. Yet, we caution that the subtle changes at 240 and 570

nm that are seen in the UV–vis spectra may influence the extent of SHG resonance enhancement.

Figure 5B shows that the interaction of the particles is largely irreversible at all particle concentrations studied in SHG experiments, at least over the time frames surveyed. Trends in the SHG intensity may be attributed to slight systematic drifts in the laser pulse energy, which were minimized by maintaining the incident pulse energy to within 2.5% of 0.4 μJ before and after recording each SHG vs time trace and monitored by recording the SHG intensity from a nonlinear crystal, potassium dihydrogen phosphate (KDP) turned to its phase-matching angle, simultaneously with the experiments.

III.F. Controls in the Presence of AuNPs. Given that the measurements we report here are the first SHG studies tracking AuNPs interacting with supported lipid bilayers, we briefly discuss control experiments to assess whether the signals recorded at 300 nm were indeed due to second harmonic generation, as opposed to fluorescence or other processes produced by the particles. Figure 5C shows no evidence for fluorescence entering the photomultiplier, and the spectral bandwidth corresponds to the second harmonic of a 120 fs input pulse at a fundamental wavelength of 612 nm. Any departure from a symmetric line shape is attributed to pulse chirping. Figure 5D shows that the SHG intensity depends quadratically on the incident pulse energy, as expected for SHG.[62] Finally, Figure 5E shows that the SHG signal is well polarized along the surface normal under our experimental conditions. Additional control experiments (Figure S14) show that the free PAH ligands held at concentrations equivalent to those expected to be representative of the nanoparticles do not produce appreciable changes in the SHG or SFG intensity when they interact with the bilayers (or the plain fused silica substrate) at 0.1 M NaCl and 0.01 M Tris buffer.

III.G. Nanoparticles Interact with Suspended Vesicles. Prior to carrying additional experiments on the supported lipid bilayers, we wanted to evaluate whether the positively and negatively charged particles interacted similarly in the absence of the SiO_2 substrate and whether any changes occurred in the chemical environment of the lipids and the ligands upon attachment. We therefore carried out a set of ^{1}H NMR experiments in which we exposed gold metal nanoparticles to suspensions of vesicles prepared from the lipids used to prepare the supported lipid bilayers. While NMR is highly sensitive to changes in the chemical environment through the chemical shift tensor, it requires fairly high concentrations, which is why we used vesicles in solution. The resonances of surface-bound ligands have characteristic features: relative to free ligands, bound ligands typically display broadened line widths (a result of decreased relaxation times) and upfield chemical shifts.[65−69] From the presence or absence of these features, we extracted molecular-level information about changes in surface chemistry as the particles interact with the lipid vesicles.

Lipid vesicle chemical shifts were assigned as shown in Figure 6. The lipid vesicles feature three prominent broad peaks for the headgroup ($-N-CH_3$, 3.15 ppm) and aliphatic ($-CH_2-$, 1.20 ppm, and $-R-CH_3$, 0.80 ppm) protons. The MPA-functionalized AuNPs exhibit narrow NMR peaks that are typical for small molecules freely tumbling in solution, such as MPA detached from the NPs. MPA is a short enough ligand (and all its protons are located sufficiently close to the NP core) that any resonances from attached MPA are almost certainly broadened beyond detection, and we would not expect to see them in the spectrum. Given that we expect some
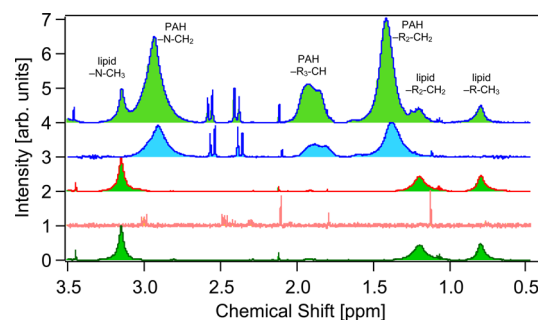

Figure 6. Normalized proton NMR spectra of (bottom to top) vesicles formed from a mixture of 9:1 DOPC:DOTAP, MPA-AuNPs, MPA-AuNPs interacting with vesicles formed from a mixture of 9:1 DOPC:DOTAP, PAH-AuNPs, and PAH-AuNPs interacting with vesicles formed from a mixture of 9:1 DOPC:DOTAP. All measurements carried out at room temperature and in 0.1 M NaCl and pH 7.4 (0.01 M Tris). See text for details.

free ligand to be in solution, it is likely that the narrow resonance peaks in the MPA-AuNP spectrum arise from this small amount of detached MPA (the low signal-to-noise ratio points to how small this amount is). It is clear that MPA is attached to the gold because the particles would not be stable or well-dispersed without that passivating layer. Finally, the PAH-wrapped AuNPs show citrate signatures near 2.5 ppm and broadened NMR features consistent with the presence of bound PAH ligand.

The 9:1 DOPC:DOTAP vesicles (12 mM) were first allowed to interact with free PAH (10 nM) for 2 h in Tris buffer in D_2O (0.1 M NaCl, 0.01 M Tris, pD 7−8), at which point NMR spectra were acquired. If the particle or polymer were to attach to the outer surface of the liposome, one would expect the lipid signals—particularly those of the headgroup protons—to broaden or shift. Alternatively, if the liposome were to fragment, mobilization of the aliphatic chains should give rise to sharper peaks. Yet, the chemical shifts and line widths of the lipid peaks remain the same, suggesting that the liposome does not undergo substantial changes in morphology or surface chemistry upon interaction with the free PAH ligand.

The 9:1 DOPC:DOTAP vesicles (12 mM) were then allowed to interact with PAH-AuNPs (10 nM) and MPA-AuNPs (10 nM) particles for 2 h in Tris buffer in D_2O (0.1 M NaCl, 0.01 M Tris, pD 7−8), at which point the NMR spectra were acquired. Figure 6 shows that the NMR response of the DOPC:DOTAP vesicles barely changes upon interaction with the MPA-AuNPs. In contrast, when the PAH-AuNPs interact with DOPC:DOTAP vesicles, the NMR signals from the chain group methylene group (1.38 ppm), chain group methine group (1.85 ppm), and side group methylene group (2.91 ppm) shift downfield by 0.02−0.03 ppm and appear between those of free PAH (shown in the Supporting Information) and the PAH-AuNPs. This response is consistent with the notion that the surface-bound PAH loosens its attachment to the particle upon contact with the lipid vesicles, more resembling free PAH, at least in terms of what is measured in NMR. Meanwhile, we find that the lipid vesicle itself is not structurally affected.

III.H. Apparent Free Energies of Particle Attachment. Having verified qualitatively similar behavior for MPA- and PAH-coated particles interacting with vesicle suspensions and supported lipid bilayers, we returned to the supported lipid bilayers, as that system enables us to probe binding interactions
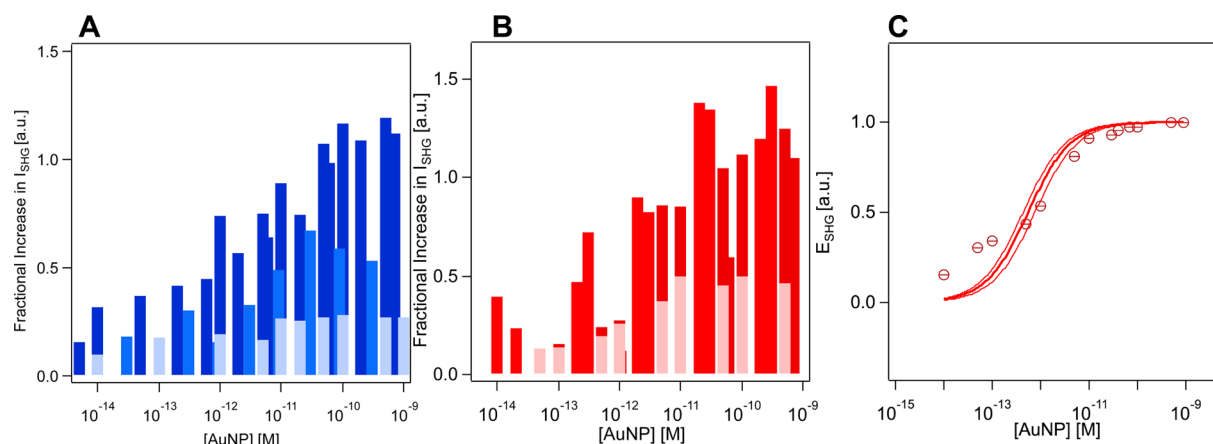
Figure 7. SHG intensity as a function of nanoparticle concentration for a supported lipid bilayer formed from a 9:1 mixture of DOPC and DOTAP upon exposure to positively charged PAH-AuNPs (A) and negatively charged MPA-AuNPs (B) at 0.001 M (dark blue and red), 0.01 M (blue and red), and 0.1 M (light blue and red) NaCl. *p*-in/all-out polarization combination, λ_{SHG} = 306 nm, and 0.01 M Tris buffer. Uncertainties on each SHG E-field is below 1% as given by the Poisson statistics of photon counting. (C) SHG E-field normalized to the maximum E-field at high particle concentration and referenced to zero particle concentration for 4 nm AuNPs coated with negatively charged MPA ligands recorded at 0.01 M Tris buffer, pH 7.4, 298 K, and 0.1 M NaCl. The solid lines represent a fit of the Langmuir adsorption model to the experimental data, specifically $\theta = K_L C/(1+ K_L C)$, where K_L is the apparent equilibrium attachment constant, C is the particle concentration, and θ is the relative SHG E-field. The thin lines indicate the upper and lower bounds of the Langmuir adsorption isotherm fit based on the uncertainty in the equilibrium constant.

without the need for quantitative separations or competitive binding assays. Specifically, we proceeded to assess the role of ionic strength on the interaction of the PAH- and MPA-AuNPs with supported lipid bilayers prepared from 9:1 mixtures of DOPC/DOTAP by recording SHG adsorption isotherms at 0.001, 0.01, and 0.1 M NaCl. As shown in Figure 7A, ionic strength plays a role in this interaction in terms of SHG signal intensities: we observed larger increases in I_{SHG} with increasing concentrations of PAH-AuNPs at lower vs at higher ionic strength, indicative of a larger amount of attachment of the PAH-AuNPs to the bilayer at low ionic strength. This result points to the importance of the hydrodynamic particle diameter in determining particle surface coverages at a given ionic strength. Figure 7 also shows that the inflection points in the adsorption isotherms occur, within an order of magnitude, at similar particle concentrations for all ionic strengths and ligand–particle combinations surveyed. This finding indicates that the apparent free energy of attachment per mole of particles is largely independent of ionic strength and ligand identity, again for the conditions surveyed.

To provide a rough estimate of the interaction energy, we fit our SHG data for the MPA-AuNPs interacting with the 9:1 DOPC:DOTAP supported lipid bilayer at 0.1 M salt to the standard Langmuir adsorption model.[63] The SHG adsorption isotherms indicate leveling off of the SHG signal intensity at higher particle concentrations, i.e., surface coverage saturation, thereby satisfying a key model assumption. Another key assumption in the Langmuir model, however, namely reversibility, may not be met as seen by SHG (Figure 5B), at least over the time scale of our experiments. Despite the fact that this and other assumptions[63] of the Langmuir model are probably not met, even under conditions of thermal averaging of the heterogeneous nature of a fluid lipid bilayer, the model has been used previously to describe the attachment of nanoparticles[64] and proteins[65] to lipid bilayers with the rationale that the desorption rate is too slow to be measured over reasonable time scales.

In our preliminary analysis, we fit the Langmuir adsorption isotherm either to the E_{SHG} values computed by taking the

square root of the SHG intensity at various nanoparticle concentrations, subtracting the nonresonant background, and normalizing to the largest E_{SHG} value at monolayer coverage (Figure 7B,C) or to the SHG intensities (data not shown). This latter fit was performed to account for the possibility that resonantly enhanced SHG signals from 4 nm AuNPs adsorbed to supported lipid bilayers that are detected at the photon multiplier may be the incoherent portion of the SHG signal produced at the interface.[61] Just like in solution,[61,66] the AuNPs should be randomly attached to the bilayer, in which case the phase relationship among the SHG E-field produced by each particle should be random, provided that the particles are separated over distances approaching or exceeding the SHG coherence length[67] (which is likely given the particle surface coverage estimates discussed above). The fit using E-fields yielded an apparent equilibrium constant, K_L^{app}, of $(1.8 \pm 0.5) \times 10^{12}$ M^{-1} for 0.1 M NaCl, corresponding to apparent adsorption free energies of -80 ± 0.7 kJ/mol of particles attached to the supported lipid bilayer formed from the 9:1 mix of DOPC:DOTAP when using the 55.5 molarity of water as a standard state for adsorption from solution.[55] Fits obtained from the SHG intensity, I_{SHG}, as opposed to E-fields, E_{SHG}, produced equilibrium constants that are 10% smaller, with comparable confidence intervals. These energies are the observed apparent adsorption free energies, which include Coulombic and non-Coulombic interactions as well as entropic contributions from water molecules and counterions being released into the bulk during the attachment process.

To put these apparent free energies into perspective, we first consider hydrogen bonding: if we assume the strength of an average hydrogen bond to be between 15 and 25 kJ/mol, 3−5 hydrogen bonds would be involved in the interaction, if it were to be indeed Langmuirian and dominated by H-bonding. Alternatively, if van der Waals interactions, such as those between two methylene groups (~2.5 kJ/mol) of the lipids and ligands,[68] were to dominate the interaction, then 30−35 such groups would be involved. These estimates represent a first step toward quantifying how many interactions are involved when nanoparticles interact with supported lipid bilayers under the

conditions of our experiments. Departures of the recorded SHG responses from the standard Langmuir adsorption model are likely due to the irreversibility of attachment and lateral particle—particle interactions. An analysis of such interactions requires high-quality adsorption isotherms, which are unfortunately not produced by this system, even from triplicate measurements. We emphasize again that the inflection points in the recorded adsorption isotherms occur at similar particle concentrations for all ionic strengths and ligand—particle combinations surveyed, indicating that the apparent free energy of attachment per mole of particles is largely independent of ionic strength and ligand identity for the conditions surveyed.

III.J. Estimating the Charge per Attached Nanoparticle. To further assess whether the MPA- and the PAH-AuNPs are charged when they attach to the lipid bilayer and to learn about the importance of Coulombic interactions in addition to a possible role of H-bonding, we carried out charge screening experiments on the attached particles. In these experiments, we change the NaCl concentration while monitoring the SHG signal intensity at constant nanoparticle concentration, which should maintain conditions of constant particle coverage according to the irreversible attachment of AuNPs to the bilayers (Figure 5B). Figure 8 shows the salt-
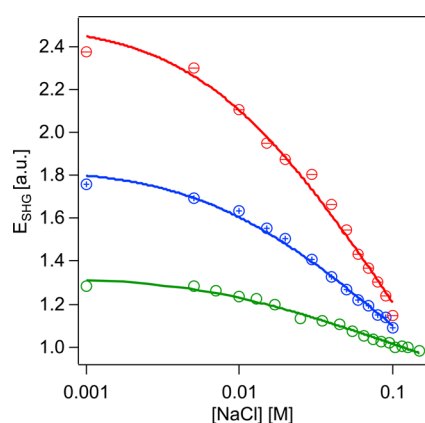

Figure 8. Normalized SHG response (symbols) as a function of NaCl concentration at pH 7.4 and 0.01 M Tris buffer for bilayers prepared from 9:1 mixtures of DOPC and DOTAP (green ○) in the presence of 1 nM 4 nm AuNPs coated with PAH (blue ⊕) ligands or MPA (red ⊖), referenced to the SHG E-field obtained at 0.1 M NaCl and in the absence of nanoparticles. Solid lines are best fit of a Gouy—Chapman model to the data. Each value is calculated as described in the Supporting Information.

dependent SHG response obtained from a supported lipid bilayer formed from a 9:1 mixture of DOPC/DOTAP maintained at 0.1 M NaCl and 0.01 M Tris buffer and subsequently exposed to 1 nM MPA- and PAH-AuNPs relative to the signal intensity obtained from the bilayer at the same salt and buffer conditions. Decreases in the salt concentration result in SHG intensity gains, consistent with the $\chi^{(3)}$ effect. Assuming the aggregation state and the optical properties of the particles attached to the bilayers are invariant with ionic strength over the course of the experiment, we fit a Gouy—Chapman model to the SHG field vs NaCl concentration data.

When expressing the total charge density additively by summing the fused silica charge density, the TrisH$^+$ charge density, the DOPC/DOTAP bilayer charge density, and the nanoparticle charge density, fit parameters with errors that were 2−10 times larger than the point estimates were obtained for

the PAH-AuNPs, indicating the total charge density (bilayer plus particles) ranges somewhere between −0.06 and +0.02 C/m^2. The Gouy—Chapman model analysis is based on mean field theory, and the charge density term for the nanoparticles yields the net number of Coulombs per m^2 associated with all particles present, irrespective of how many particles are present (e.g., not the charge per nanoparticle). Computing the charge density per nanoparticle requires knowledge of how many particles are present per m^2. QCM-D experiments conducted at 1 nM PAH-AuNP indicate roughly 1×10^{11} particles attached per cm^2, which is an upper bound as the mass sensed by QCM-D includes hydrodynamically coupled water. After taking into account the bilayer charge density (−0.015 (+0.003/−0.004) C/m^2), the total charge density per PAH-AuNP is estimated from the Gouy—Chapman model fit to be between -4.5×10^{-17} and $+3.5 \times 10^{-17}$ C; i.e., they are associated with anywhere between approximately 200 positive or 200 negative charges.

To understand this finding, we consider the following: the independent measurements of adsorption isotherms recorded at varying salt concentrations (section III.H) and of charge screening experiments (section III.J) highlight how important counterions are for the PAH-AuNP system studied here. Specifically, the ~+30 mV zeta potentials we obtain for the PAH-AuNPs in solution indicate some amount of net positive charge associated with the particles at the zeta plane. The PAH molecular mass is ~15 000 g/mol, with the allylamine repeat unit having a molecular mass of 57 g/mol. XPS analysis indicated an average of four PAH polymers per particle. From this result we calculate that approximately 1000 positive charges are available on average at the particle surface, assuming full ionization of the ammonium group at pH 7.4. Similar to reports that micelles formed at ~500 mM ionic strength from cetyltrimethylammonium bromide and chloride carry 71% and 55% of their cationic charge as counterions,[69] and similar to reports that condensed counterions are key to forming DNA duplexes,[70−78] origami,[79,80] colloidal crystals,[81−83] and even spherical nucleic acids[84,85] from otherwise highly charged single strands, the PAH-AuNPs studied here are likely to contain condensed (i.e., strongly coordinated) counterions that substantially reduce the effective charge density. Upon attachment to the supported lipid bilayer, interaction with the negatively charged phosphate groups in the PC headgroups, and/or any negatively charged counterions associated with the electrical double layer above them, appears to reduce the net charge of the attached particles even further to somewhere between 200 hundred positive or 200 negative charges per particle. An estimate of the number of lipid headgroups that may provide, either by themselves or by means of associated counterions, negative charge to the attached particle is possible by calculating, from the lipid density reported in section III.A, the number of lipids located within the footprint of the attached particle, which we assume to be 26 nm^2 based on the hydrodynamic radii for these particles at 0.001 M NaCl (section II.B). This calculation yields 100−200 lipids and/or associated counterions with them that are in close proximity to the attached particle, clearly in the range to allow for nearly quantitative charge neutralization of the particle. We emphasize that the range of charges per attached particle includes charge contributions from any charged species located within the hydrodynamic volume, provided they are in the SHG active region of the interface.

In contrast to the positively charged PAH-AuNPs, the surface coverage of the negatively charged MPA-AuNPs is estimated to be less than 0.01 ng/cm^2 particles, or just 1×10^7 AuNPs per cm^2, the lower end of our estimated XPS detection limit. Yet, the interfacial charge density we obtain from fitting the Gouy–Chapman model to the charge screening data shown in Figure 8 ranges between −0.05 and −0.01 C/m^2 for the MPA-AuNP-containing supported lipid bilayer, which is largely indistinguishable from the −0.06 and +0.02 C/m^2 charge density obtained from the PAH-AuNP-containing supported lipid bilayer. With a detection limit of better than 3×10^{-4} C/m^2 under similar aqueous phase conditions,[86] the SHG $\chi^{(3)}$ method should be appropriate for determining 10^9 charged MPA-coated particles per cm^2. (This estimate assumes the MPA particles carry the same net 200 elementary charges as the PAH-coated particles, which is reasonable, at least within an order of magnitude, given the similar magnitudes in zeta potential of the two particles types studied here at 0.1 M NaCl concentration.) Yet, the MPA-AuNP coverages is estimated to be just 1×10^7 particles/cm^2, pointing to the possibility that the attached MPA-AuNPs carry a much larger net negative charge than the attached PAH-AuNPs or that the charge per particle is too small to be evaluated using Gouy–Chapman theory. The small surface coverage we estimate for the MPA-AuNPs appears to support, at least given the current set of data, the former case, i.e., much larger charge density per attached MPA-coated particles than per PAH-coated particle. This outcome of our analysis is readily understood when considering that the MPA- and PAH-AuNPs exhibit hydrodynamic diameters of 250 and 70 nm, respectively, at 0.1 M NaCl concentration, corresponding to a ~50-fold increase in volume for the MPA-coated particles to carry condensed, i.e., strongly bound, ions for repelling like charges. Our findings thus points toward a mechanism in which the attachment of MPA- and PAH-AuNPs is controlled by the hydrodynamic volume and the number of charges within it.

IV. SUMMARY AND CONCLUSIONS

In summary, we have presented the first comprehensive, multiprobe molecular-level investigation of the nano–bio interface that focuses on the lipids of the bilayer, the metal core of the nanoparticles, and the role of molecular structure, electrostatics, and ionic strength in mediating the interactions between bilayers and nanoparticles. First, we prepared well-characterized supported lipid bilayers. Next, we carried out the first label-free determination of the interfacial charge densities and potentials of supported lipid bilayers by means of nonlinear optics. Third, we demonstrated the applicability of second harmonic generation for following the interaction of positively and negatively charged AuNP cores with supported lipid bilayers under varying nanoparticle concentrations, while paying particular attention to the role of bilayer order and disorder, as well as electrostatics of the bilayers and the particles. Special attention was paid to control experiments ruling out, within the constraints of our experiments, exogenous effects and to carrying out complementary studies using NMR, QCM-D, AFM, XPS, FRAP, and ToF-SIMS.

While avoiding overinterpretation of our experimental data and the models we apply to analyze them, the data set we have presented is consistent with an apparent negative charge density of 1.8 ± 0.5% of an elementary negative charge for zwitterionic PC head groups in supported lipid bilayers. Depending on the salt concentration, we found that PC-rich

supported lipid bilayers are associated with sizable negative interfacial potentials, irrespective of if they contained minority components of positively or negatively charged lipids. Structural changes within the alkyl tails of the lipids constituting the bilayers, probed in the C–H stretching region using vibrational sum frequency generation, were found to be negligible for salt concentrations between 0.001 and 0.1 and 0.01 M Tris buffer.

We then quantified the extent and reversibility of nanoparticle–bilayer interactions by recording resonantly enhanced SHG signals at 0.1 M NaCl and 0.01 M Tris buffer as a function of AuNP concentration between 10^{-14} and 10^{-9} M. A combination of nonlinear optics, XPS, QCM-D, AFM, and ToF-SIMS indicates that the supported lipid bilayers interact with positively and negatively charged particles at 0.1 M NaCl. Complementary studies of DOPC/DOTAP vesicles suspended in 0.1 M NaCl and 0.01 M Tris buffer showed their NMR spectra change little, if at all, upon interaction with the MPA-AuNPs. In contrast, NMR spectra are consistent with loosening of the gold-bound PAH polymer wrapping upon attachment to the lipid vesicles, while the lipid vesicles themselves are not structurally affected.

From PAH-AuNP adsorption isotherms recorded using DOPC/DOTAP supported lipid bilayers we calculated apparent adsorption free energies of approximately −80 kJ/mol at 0.1 M salt concentration. The adsorption isotherms appear to be independent of ionic strength, i.e., interfacial potential. QCM-D indicates 1×10^{11} PAH-AuNPs are attached per cm^2 at 1 nM particle concentration and 0.1 M salt concentration. Resonantly enhanced SHG signals are larger at 0.001 M vs 0.1 M salt concentration. SHG charge screening experiments carried out on the attached PAH-AuNPs indicate the presence of about 200 negative or positive charges, which are likely to be distributed over the hydrodynamic volume of each attached particle. We propose that the two main contributors to determining the thermodynamics and coverage of PAH-coated, 4 nm AuNPs are (1) multivalent van der Waals or hydrogen bonding interactions, which contribute an apparent free energy gain of −80 kJ per mol of adsorbing particles that seem to be largely invariant with ionic strength, (2) the hydrodynamic diameter of the adsorbing particles, which is smaller at low ionic strength than at high ionic strength, a result that reflects the higher SHG signal intensities observed at low vs high ionic strength, and (3) charge–charge repulsion among the attached PAH-AuNPs, which limits the surface coverage to the saturation levels observed in the SHG isotherms.

Unlike the PAH-AuNPs, the attached MPA-AuNPs are likely to be associated with larger charge densities at 0.1 M NaCl, which includes counterions and any other charged species present within the hydrodynamic volume. Even though only ~1 $\times 10^7$ MPA-AuNPs attach to the supported lipid bilayer, the SHG signals produced by the former are sizable, pointing to an in-phase, or constructive, interference between the resonantly enhanced and potential-dependent SHG terms. Deconstructive interference between the two terms probably suppresses SHG signal intensities in the case of the PAH-AuNPs, which produce less SHG signal intensity even though their surface coverages are several orders of magnitude above those we estimate for the MPA-AuNPs.

The quantitative results presented here may serve as important benchmarks for computational and experimental studies of lipid bilayers and may serve to calibrate interaction

potentials and spectrochemical labels. As an example, the apparent independence of the ΔG_{obs}^{app} value reported here for the MPA-AuNPs interacting with the DOPC:DOTAP bilayer indicates it is in fact the chemical interaction free energy, with any influences from Coulombic interactions being largely negligible. This result will be useful in atomistic simulations of how PAH-AuNPs may interact with bilayers. The findings presented here may also allow predictions of how charged species interact with lipid membranes rich in phosphatidylcholine headgroups. The results from our study open the possibility for future work aimed at elucidating the interplay between resonant and nonresonant SHG from charged AuNPs, testing how applicable our findings are to other particle/ligand/lipid combinations, surveying particle−bilayer interactions for bilayers containing not just lipids but also other components known to be important in biological membranes, such as lipopolysaccharides, and focusing on the effects of particle size and core composition on the interaction of nanoparticles with supported lipid bilayers.

■ ASSOCIATED CONTENT

ⓢ Supporting Information

Details regarding the experiments, fitting procedures, sample preparation and characterization, and negative controls. This material is available free of charge via the Internet at http://pubs.acs.org.

■ AUTHOR INFORMATION

Corresponding Authors

*E-mail joelpedersen@wisc.edu (J.A.P.).
*E-mail geigerf@chem.northwestern.edu (F.M.G.).

Present Address

S.R.W.: Department of Chemistry of Tufts University, 62 Talbot Avenue, Medford, MA 02155.

Notes

The authors declare no competing financial interest.

■ ACKNOWLEDGMENTS

■ REFERENCES

(1) Mueller, P.; Rudin, D. O.; Tien, H. T.; Wescott, W. C. Reconstitution of Cell Membrane Structure in Vitro and Its Transformation into an Excitable System. *Nature* **1962**, *194*, 979−980.

(2) MacDonald, R. C.; Bangham, A. D. Comparison of Double Layer Potentials in Lipid Monolayers and Lipid Bilayer Membranes. *J. Membr. Biol.* **1972**, *7*, 29−53.

(3) Sackmann, E. Supported Membranes: Scientific and Practical Applications. *Science* **1996**, *271*, 43−48.

(4) Voet, D.; Voet, J. G. *Biochemistry*, 3rd ed.; Wiley Text Books: New York, 2004.

(5) Schwarzenbach, R.; Geschwend, P. M.; Imboden, D. M. *Environmental Organic Chemistry*; John Wiley & Sons: New York, 1993.

(6) Boxer, S. G. Molecular Transport and Organization in Supported Lipid Membranes. *Curr. Opin. Chem. Biol.* **2000**, *4*, 704−709.

(7) Nel, A. E.; Madler, L.; Velegol, D.; Xia, T.; Hoek, E. M. V.; Somasundaran, P.; Klaessig, F.; Castranova, V.; Thompson, M. Understanding Biophysicochemical Interactions at the Nano-Bio Interface. *Nat. Mater.* **2009**, *8*, 543−557.

(8) Gagner, J. E.; Shrivastava, S.; Qian, X.; Dordick, J. S.; Siegel, R. W. Engineering Nanomaterials for Biomedical Applications Requires Understanding the Nano-Bio Interface: A Perspective. *J. Phys. Chem. Lett.* **2012**, *3*, 3149−3158.

(9) Yang, Y.; Mayer, K. M.; Wickremasinghe, N. S.; Hafner, J. H. Probing the Lipid Membrane Dipole Potential by Atomic Force Microscopy. *Biophys. J.* **2008**, *95*, 5193−5199.

(10) Poyton, M. F.; Cremer, P. S. Electrophoretic Measurements of Lipid Charges in Supported Bilayers. *Anal. Chem.* **2013**, *85*, 10803−10811.

(11) Karaoka-Hamai, C.; Inoue, H.; Miyahara, Y. Detection of Supported Lipid Bilayers Using Their Electric Charge. *Langmuir* **2008**, *24*, 9916−9920.

(12) Van Lehn, R. C.; Ricci, M.; Silca, P. H. C.; Adndreozzi, P.; Reguera, J.; Voichovsky, K.; Stellacci, F.; Alexander-Katz, A. Lipid Tail Protrusions Mediate the Insertion of Nanoparticles into Model Cell Membranes. *Nat. Commun.* **2014**, *5*, 2−11.

(13) Zhang, X.; Yang, S. Nonspecific Adsorption of Charged Quantum Dots on Supported Zwitterionic Lipid Bilayers: Real-Time Monitoring by Quartz Crystal Microbalance with Dissipation. *Langmuir* **2011**, *27*, 2528−2535.

(14) Yi, P.; Chen, K. L. Interaction of Multiwalled Carbon Nanotubes with Supported Lipid Bilayers and Vesicles as Model Biological Membranes. *Environ. Sci. Technol.* **2013**, *47*, 5711−5719.

(15) Xi, A. H.; Bothun, G. D. Centrifugation-Based Assay for Examining Nanoparticle-Lipid Membrane Binding and Disruption. *Analyst* **2014**, *139*, 973−981.

(16) Lee, Y. K.; Kim, S.; Oh, J.-W.; Nam, J.-M. Massively Parallel and Highly Quantitative Single-Particle Analysis on Interactions between Nanoparticles on Supported Lipid Bilayer. *J. Am. Chem. Soc.* **2014**, *136*, 4081−4088.

(17) Roiter, Y.; Ornatska, M.; Rammohan, A. R.; Balakrishnan, J.; Heine, D. R.; Minko, S. Interaction of Nanoparticles with Lipid Membrane. *Nano Lett.* **2008**, *8*, 941−944.

(18) Jain, P. K.; Huang, X. H.; El-Sayed, I. H.; El-Sayed, M. A. Noble Metals on the Nanoscale: Optical and Photothermal Properties and Some Applications in Imaging, Sensing, Biology, and Medicine. *Acc. Chem. Res.* **2008**, *41*, 1578−1586.

(19) Murphy, C. J.; Gole, A. M.; Stone, J. W.; Sisco, P. N.; Alkilany, A. M.; Goldsmith, E. C.; Baxter, S. C. Gold Nanoparticles in Biology: Beyond Toxicity to Cellular Imaging. *Acc. Chem. Res.* **2008**, *41*, 1721−1730.

(20) Yeagle, P. L. *The Membranes of Cells*; Academic Press: Boston, 1993.

(21) Castellana, E. T.; Cremer, P. S. Solid Supported Lipid Bilayers: From Biophysical Studies to Sensor Design. *Surf. Sci. Rep.* **2006**, *61*, 429−444.

(22) Voinova, M. V.; Rodahl, M.; Johnson, M.; Kasemo, B. Viscoelastic Acoustic Response of Layered Polymer Films at Fluid-Solid Interfaces: Continuum Mechanics Approach. *Phys. Scr.* **1999**, *59*, 391.

(23) Malin, J. N.; Hayes, P. L.; Geiger, F. M. Interactions of Ca, Zn, and Cd Ions at Buried Solid/Water Interfaces Studied by Second Harmonic Generation. *J. Phys. Chem. C* **2008**, *113*, 2041−2052.

(24) Hayes, P. L.; Chen, E. H.; Achtyl, J. L.; Geiger, F. M. An Optical Voltmeter for Studying Cetyltrimethylammonium Interacting with Fused Silica/Aqueous Interfaces at High Ionic Strength. *J. Phys. Chem. A* **2009**, *113*, 4269−4280.

(25) Hayes, P. L.; Gibbs-Davis, J. M.; Musorrafiti, M. J.; Mifflin, A. L.; Scheidt, K. A.; Geiger, F. M. Environmental Biogeochemistry Studied

by Second-Harmonic Generation: A Look at the Agricultural Antibiotic Oxytetracycline. *J. Phys. Chem. C* **2007**, *111*, 8796−8804.

(26) Konek, C. T.; Illg, K. D.; Al-Abadleh, H. A.; Voges, A. B.; Yin, G.; Musorrafiti, M. J.; Schmidt, C. M.; Geiger, F. M. Nonlinear Optical Studies of the Agricultural Antibiotic Morantel Interacting with Silica/Water Interfaces. *J. Am. Chem. Soc.* **2005**, *127*, 15771−15777.

(27) Brust, M.; Walker, M.; Bethell, D.; Schiffrin, D. J.; Whyman, R. Synthesis of Thiol-Derivatized Gold Nanoparticles in a 2-Phase Liquid-Liquid System. *J. Chem. Soc., Chem. Commun.* **1994**, 801−802.

(28) Sweeney, S. F.; Woehrle, G. H.; Hutchison, J. E. Rapid Purification and Size Separation of Gold Nanoparticles via Diafiltration. *J. Am. Chem. Soc.* **2006**, *128*, 3190−3197.

(29) Jana, N. R.; Gearheart, L.; Murphy, C. J. Seeding Growth for Size Control of 5−40 nm Diameter Gold Nanoparticles. *Langmuir* **2001**, *17*, 6782−6786.

(30) Gole, A.; Murphy, C. J. Polyelectrolyte-Coated Gold Nanorods: Synthesis, Characterization and Immobilization. *Chem. Mater.* **2005**, *17*, 1325−1330.

(31) Haiss, W.; Thanh, N. T. K.; Aveyard, J.; Fernig, D. G. Determination of Size and Concentration of Gold Nanoparticles from UV-Vis Spectra. *Anal. Chem.* **2007**, *79*, 4215−4221.

(32) Woehrle, G. H.; Hutchison, J. E.; Ozkar, S.; Finke, R. G. Analysis of Nanoparticle Transmission Electron Microscopy Data Using a Public-Domain Image-Processing Program, Image. *Turk. J. Chem.* **2006**, *30*, 1−13.

(33) Zwang, T. J.; Fletcher, W. R.; Lane, T. J.; Johal, M. S. Quantification of the Layer of Hydration of a Supported Lipid Bilayer. *Langmuir* **2010**, *26*, 4598.

(34) Cho, N. J.; Frank, C. W.; Kasemo, B.; Hook, F. Quartz Crystal Microbalance with Dissipation Monitoring of Supported Lipid Bilayers on Various Substrates. *Nat. Protoc.* **2010**, *5*, 1096−1106.

(35) Richter, R. P.; Berat, R.; Brisson, A. R. Formation of Solid-Supported Lipid Bilayers: An Integrated View. *Langmuir* **2006**, *22*, 3497−3505.

(36) Richter, R. P.; Brisson, A. R. Characterization of Lipid Bilayers and Protein Assemblies Supported on Rough Surfaces by Atomic Force Microscopy. *Langmuir* **2003**, *19*, 1632−1640.

(37) Hamai, C.; Yang, T. L.; Kataoka, S.; Cremer, P. S.; Musser, S. M. Effect of Average Phospholipid Curvature on Supported Bilayer Formation on Glass by Vesicle Fusion. *Biophys. J.* **2006**, *90*, 1241−1248.

(38) Hamai, C.; Cremer, P. S.; Musser, S. M. Single Giant Vesicle Rupture Events Reveal Multiple Mechanisms of Glass-Supported Bilayer Formation. *Biophys. J.* **2007**, *92*, 1988−1999.

(39) Lapinski, M. M.; Castro-Forero, A.; Greiner, A. J.; Ofoli, R. Y.; Blanchard, G. J. Comparison of Liposomes Formed by Sonication and Extrusion: Rotational and Translational Diffusion of an Embedded Chromophore. *Langmuir* **2007**, *23*, 11677−11683.

(40) Cho, N. J.; Hwang, L. Y.; Solandt, J. J. R.; Frank, C. W. Comparison of Extruded and Sonicated Vesicles for Planar Bilayer Self-Assembly. *Materials* **2013**, *6*, 3294−3308.

(41) Zhao, X.; Ong, S.; Wang, H.; Eisenthal, K. B. New Method for Determination of Surface Pka Using Second Harmonic Generation. *Chem. Phys. Lett.* **1993**, *214*, 203−207.

(42) Yan, E. C. Y.; Liu, Y.; Eisenthal, K. B. New Method for Determination of Surface Potential of Microscopic Particles by Second Harmonic Generation. *J. Phys. Chem. B* **1998**, *102*, 6331−6336.

(43) Kasbauer, M.; Junglas, M.; Bayerl, T. M. Effect of Cationic Lipids in the Formation of Asymmetries in Supported Bilayers. *Biophys. J.* **1999**, *76*, 2600−2605.

(44) Shreve, A. P.; Howland, M. C.; Sapuri-Butti, A. R.; Allen, T. W.; Parikh, A. N. Evidence for Leaflet-Dependent Redistribution of Charged Molecules in Fluid Supported Phospholipid Bilayers. *Langmuir* **2008**, *24*, 13250−13253.

(45) Hayes, P. L.; Malin, J. N.; Jordan, D. S.; Geiger, F. M. Get Charged Up: Nonlinear Optical Voltammetry for Quantifying the Thermodynamics and Electrostatics of Metal Cations at Aqueous/Oxide Interfaces. *Chem. Phys. Lett.* **2010**, *499*, 183−192.

(46) Sauerbeck, C.; Braunschweig, B.; Peukert, W. Surface Charging and Interfacial Water Structure of Amphoteric Colloidal Particles. *J. Phys. Chem. C* **2014**, *118*, 10033−10042.

(47) Stack, A. G.; Higgins, S. R.; Eggleston, C. M. Point of Zero Charge of a Corundum-Water Interface Probed with Optical Second Harmonic Generation (SHG) and Atomic Force Microscopy (AFM): New Approaches to Oxide Surface Charge. *Geochim. Cosmochim. Acta* **2001**, *65*, 3055−3063.

(48) Shiratori, K.; Yamaguchi, S.; Tahara, T.; Morita, A. Computational Analysis of the Quadrupole Contribution in the Second-Harmonic Generation Spectroscopy for the Water/Vapor Interface. *J. Chem. Phys.* **2013**, *138*, 064704.

(49) Chen, X.; Hua, W.; Huang, Z.; Allen, H. C. Interfacial Water Structure Associated with Phospholipid Membranes Studied by Phase-Sensitive Vibrational Sum Frequency Generation Spectroscopy. *J. Am. Chem. Soc.* **2010**, *132*, 11336−11342.

(50) Mondal, J. A.; Nihongyanagi, S.; Yamaguchi, S.; Tahara, T. Three Distinct Water Structrues at a Zwitterionic Lipid/Water Interface Revealed by Heterodyne-Detected Vibrational Sum Frequency Generation. *J. Am. Chem. Soc.* **2012**, *134*, 7842−7850.

(51) Nagata, Y.; Mukamel, S. Vibrational Sum-Frequency Generation Spectroscopy at the Water/Lipid Interface: Molecular Dynamics Simulation Study. *J. Am. Chem. Soc.* **2010**, *132*, 6434−6442.

(52) Zimmermann, R.; Küttner, D.; Renner, L.; Kaufmann, M.; Zitzmann, J.; Müller, M.; Werner, C. Charging and Structure of Zwitterionic Supported Bilayer Lipid Membranes Studied by Streaming Current Measurements, Fluorescence Microscopy, and Attenuated Total Reflection Fourier Transform Infrared Spectroscopy. *Biointerphases* **2009**, *4*, 1−6.

(53) Voinov, M. A.; Rivera-Rivera, I.; Smirnov, A. I. Surface Electrostatics of Lipid Bilayers by EPR of a pH-Sensitive Spin-Labeled Lipid. *Biophys. J.* **2013**, *104*, 106−116.

(54) Peitzsch, R. M.; Eisenberg, M.; Sharp, K. A.; McLaughlin, S. Calculations of the Electrostatic Potential Adjacent to Model Phospholipid Bilayers. *Biophys. J.* **1995**, *68*, 729−738.

(55) Adamson, A. W. *Physical Chemistry of Surfaces*, 5th ed.; John Wiley & Sons: New York, 1990.

(56) Hayes, P. L.; Malin, J. N.; Konek, C. T.; Geiger, F. M. Interaction of Nitrate, Barium, Strontium and Cadmium Ions with Fused Quartz/Water Interfaces Studied by Second Harmonic Generation. *J. Phys. Chem. A* **2008**, *112*, 660−668.

(57) Achtyl, J. L.; Vlassiouk, I. V.; Fulvio, P. F.; Mahurin, S. M.; Dai, S.; Geiger, F. M. Free Energy Relationships in the Electrical Double Layer over Single-Layer Graphene. *J. Am. Chem. Soc.* **2013**, *135*, 979−981.

(58) Nagle, J. F.; Tristram-Nagle, S. Structure of Lipid Bilayers. *Biochim. Biophys. Acta* **2000**, *1469*, 159−195.

(59) Dreaden, E. C.; Alkilany, A. M.; Huang, X. H.; Murphy, C. J.; El-Sayed, M. A. The Golden Age: Gold Nanoparticles for Biomedicine. *Chem. Soc. Rev.* **2012**, *41*, 2740−2779.

(60) Sandrock, M. L.; Pibel, C. D.; Geiger, F. M.; Foss, C. A. Synthesis and Second-Harmonic Generation Studies of Noncentrosymmetric Gold Nanostructures. *J. Phys. Chem. B* **1999**, *103*, 2668−2673.

(61) Eisenthal, K. B. Second Harmonic Spectroscopy of Aqueous Nano- and Microparticle Interfaces. *Chem. Rev.* **2006**, *106*, 1462−1477.

(62) Svelto, O.; Hanna, D. C. SpringerLink (Online service), *Principles of Lasers*, 5th ed.; Springer: New York, 2009; p 1 v http://turing.library.northwestern.edu/login?url=http://dx.doi.org/10.1007/978-1-4419-1302-9.

(63) Somorjai, G. A. *Chemistry in Two Dimensions*; Cornell University Press: Ithaca, NY, 1981.

(64) Carney, R. P.; Astier, Y.; Carney, T. M.; Voïtchovsky, K.; Jacob Silva, P. H.; Stellacci, F. Electrical Method to Quantify Nanoparticle Interaction with Lipid Bilayers. *ACS Nano* **2013**, *7*, 932−942.

(65) Nguyen, T. T.; Sly, K. L.; Conboy, J. C. Comparison of the Energetics of Avidin, Streptavidin, Neutravidin, and Anti-Biotin

Antibody Binding to Biotinylated Lipid Bilayer Examined by Second-Harmonic Generation. *Anal. Chem.* **2011**, *84*, 201−208.

(66) Yan, E.; Liu, Y.; Eisenthal, K. New Method for Determination of Surface Potential of Microscopic Particles by Second Harmonic Generation. *J. Phys. Chem. B* **1998**, *102*, 6331−6336.

(67) Xu, J.; Zhang, X. Second Harmonic Generation in Three-Dimensional Structures Based on Homogeneous Centrosymmetric Metallic Spheres. *Opt. Express* **2012**, *20*, 1668−1684.

(68) Atkins, P.; de Paula, J. *Physical Chemistry*, 7th ed.; W.H. Freeman and Co.: New York, 2002.

(69) Lindman, B.; Puyal, M. C.; Kamenka, N.; Rymden, R.; Stilbs, P. Micelle Formation of Anionic and Cationic Surfactants from Fourier Transform Proton and Lithium-7 Nuclear Magnetic Resonance and Tracer Self-Diffusion Studies. *J. Phys. Chem.* **1984**, *88*, 5048−57.

(70) Walter, S. R.; Young, K. L.; Holland, J. G.; Gieseck, R. L.; Mirkin, C. A.; Geiger, F. M. Counting the Number of Magnesium Ions Bound to the Surface-Immobilized Thymine Oligonucleotides That Comprise Spherical Nucleic Acids. *J. Am. Chem. Soc.* **2013**, *135*, 17339−17348.

(71) Chiu, T. K.; Dickerson, R. E. 1 Å Crystal Structures of B-DNA Reveal Sequence-Specific Binding and Groove-Specific Bending of DNA by Magnesium and Calcium. *J. Mol. Biol.* **2000**, *301*, 915−945.

(72) Hackl, E. V.; Kornilova, S. V.; Kapinos, L. E.; Andrushchenko, V. V.; Galkin, V. L.; Grigoriev, D. N.; Blagoi, Y. P. Study of Ca^{2+}, Mn^{2+} and Cu^{2+} Binding to DNA in Solution by Means of IR Spectroscopy. *J. Mol. Struct.* **1997**, *408−409*, 229−232.

(73) Duguid, J.; Bloomfield, V. A.; Benevides, J.; Thomas, G. J., Jr. Raman Spectroscopy of DNA-Metal Complexes. I. Interactions and Conformational Effects of the Divalent Cations: Mg, Ca, Sr, Ba, Mn, Co, Ni, Cu, Pd, and Cd. *Biophys. J.* **1993**, *65*, 1916−1928.

(74) Anastassopoulou, J.; Theophanides, T. Magnesium−DNA Interactions and the Possible Relation of Magnesium to Carcinogenesis. Irradiation and Free Radicals. *Crit. Rev. Oncol./Hematol.* **2002**, *42*, 79−91.

(75) Misra, V. K.; Draper, D. E. On the Role of Magnesium Ions in RNA Stability. *Biopolymers* **1998**, *48*, 113−135.

(76) Ott, G. S.; Ziegler, R.; Bauer, W. R. DNA Melting Transition in Aqueous Magnesium Salt Solutions. *Biochemistry* **1975**, *14*, 3431−3438.

(77) Owczarzy, R.; Moreira, B. G.; You, Y.; Behlke, M. A.; Walder, J. A. Predicting Stability of DNA Duplexes in Solutions Containing Magnesium and Monovalent Cations. *Biochemistry* **2008**, *47*, 5336−5353.

(78) Record, M. T. Effects of Na^+ and Mg^{++} Ions on the Helix−Coil Transition of DNA. *Biopolymers* **1975**, *14*, 2137−2158.

(79) Liu, W.; Zhong, H.; Wang, R.; Seeman, N. C. Crystalline Two-Dimensional DNA-Origami Arrays. *Angew. Chem., Int. Ed.* **2011**, *50*, 264−267.

(80) Seeman, N. C. DNA in a Material World. *Nature* **2003**, *421*, 427.

(81) Park, S. Y.; Lytton-Jean, A. K. R.; Lee, B.; Weigand, S.; Schatz, G. C.; Mirkin, C. A. DNA-Programmable Nanoparticle Crystallization. *Nature* **2008**, *451*, 553−556.

(82) Mirkin, C. A.; Letsinger, R. L.; Mucic, R. C.; Storhoff, J. J. A DNA-Based Method for Rationally Assembling Nanoparticles into Macroscopic Materials. *Nature* **1996**, *382*, 607−609.

(83) Alivisatos, A. P.; Johnson, K. P. Organization of 'Nanocrystal Molecules' Using DNA. *Nature* **1996**, *382*, 609.

(84) Cutler, J. I.; Auyeung, E.; Mirkin, C. A. Spherical Nucleic Acids. *J. Am. Chem. Soc.* **2012**, *134*, 1376−1391.

(85) Seferos, D. S.; Prigodich, A. E.; Giljohann, D. A.; Patel, P. C.; Mirkin, C. A. Polyvalent DNA Nanoparticle Conjugates Stabilize Nucleic Acids. *Nano Lett.* **2008**, *9*, 308−311.

(86) Konek, C. T.; Musorrafiti, M. J.; Al-Abadleh, H. A.; Bertin, P. A.; Nguyen, S. T.; Geiger, F. M. Interfacial Acidities, Charge Densities, Potentials, and Energies of Carboxylic Acid-Functionalized Silica/Water Interfaces Determined by Second Harmonic Generation. *J. Am. Chem. Soc.* **2004**, *126*, 11754−11755.